J Solid State Electrochem (2012) 16:375–382
DOI 10.1007/s10008-011-1326-7

ORIGINAL PAPER

Synthesis and electrochemical performances of $Li_4Ti_{4.95}Zr_{0.05}O_{12}$/C as anode material for lithium-ion batteries

Fang Gu · Gang Chen · Zhenhong Wang

Received: 17 December 2010 / Revised: 21 January 2011 / Accepted: 30 January 2011 / Published online: 25 March 2011

Abstract Spinel $Li_4Ti_{5-x}Zr_xO_{12}$/C (x=0, 0.05) were prepared by a solution method. The structure and morphology of the as-prepared samples were characterized by X-ray diffraction, scanning electron microscopy, and transmission electron microscopy. The electrochemical performances including charge–discharge (0–2.5 V and 1–2.5 V), cyclic voltammetry, and ac impedance were also investigated. The results revealed that the $Li_4Ti_{4.95}Zr_{0.05}O_{12}$/C had a relatively smaller particle size and more regular morphology than that of $Li_4Ti_5O_{12}$/C. Zr^{4+} doping enhanced the ability of lithium-ion diffusion in the electrode. It delivered a discharge capacity 289.03 mAh g^{-1} after 50 cycles for the Zr^{4+}-doped $Li_4Ti_5O_{12}$/C while it decreased to 264.03 mAh g^{-1} for the $Li_4Ti_5O_{12}$/C at the 0.2C discharge to 0 V. Zr^{4+} doping did not change the electrochemical process, instead enhanced the electronic conductivity and ionic conductivity. The reversible capacity and cycling performance were effectively improved especially when it was discharged to 0 V.

Keywords Lithium-ion battery · Anode material · $Li_4Ti_5O_{12}$/C · Zr^{4+} substitution

F. Gu · G. Chen (✉) · Z. Wang
Department of Chemistry, Harbin Institute of Technology,
Harbin 150001, China
e-mail: gchen@hit.edu.cn

F. Gu
College of Food Engineering of Harbin University
of Commerce Chemistry Center,
Harbin 150076, China

Introduction

Recently, spinel lithium titanate has been regarded as a very promising anode material for lithium secondary batteries [1, 2]. The cycle performance of traditional anode material, graphite, was generally poor and cost was high, so it could not face the demand for the development of hybrid vehicles. Compared with the currently used graphite, $Li_4Ti_5O_{12}$ had many advantages such as low cost, zero-strain structural change in the charge–discharge process [3, 4], and a stable operating voltage at approximately 1.55 V vs. lithium.

However, low electronic and lithium ionic conductivity were the main obstacles preventing $Li_4Ti_5O_{12}$ to be put into commercial use. Low conductivity would have effect on the electrochemical properties. To improve the conductivity, several effective ways have been proposed, including synthesis of nanostructured $Li_4Ti_5O_{12}$ [5–7]; substitution of a small quality of Li^+ or Ti^{4+} by supervalent metal ions (K^+ [8], Mg^{2+} [9], Zn^{2+} [10], Ni^{3+} [11], Al^{3+} [12], Cr^{3+} [13], Co^{3+} [14], Fe^{3+} [15], Mn^{3+} [16], Ga^{3+} [17], Zr^{4+} [18], Mo^{4+} [19], V^{5+} [20], Ta^{5+} [21], F^- [22], and Br^- [23]); synthesis of electronic conductor composites such as Cu [24], Ag [25], and carbon [26–28], etc. Generally, $Li_4Ti_5O_{12}$ was synthesized by solid-state reaction [20], sol–gel synthesis [29], hydrothermal synthesis [30], and so on. But solid-state reaction methods not only needed high temperature but also took a long time. Sol–gel synthesis and hydrothermal synthesis were complex. So, these methods were unsuitable for practical application. To overcome these drawbacks, solution method has been investigated to prepare $Li_4Ti_5O_{12}$ in this work.

Li et al. [18] have prepared spinel $Li_4Ti_{5-x}Zr_xO_{12}$ (x= 0, 0.05, 0.1, 0.2) by solid-state reaction; their charge–

discharge of the cells were recorded in a potential range between 1.0 and 3.0 V. As far as we know, no research has been attempted to investigate the electrochemical properties of $Li_4Ti_{5-x}Zr_xO_{12}/C$ (x=0, 0.05) discharged to 0 V. It was important to study the electrochemical behaviors of anode materials at low voltage because capacity of the anode materials at lower voltage can offer a higher cell voltage and reversible capacity for lithium-ion batteries.

In the present work, anode materials $Li_4Ti_{5-x}Zr_xO_{12}/C$ (x=0, 0.05) were synthesized with an easy solution method. In addition, low-cost $LiOH{\cdot}H_2O$ was selected as lithium source instead of expensive CH_3COOLi or $LiNO_3$, and sucrose was adopted as carbon source. The electrochemical properties of the synthesized composite powders were discussed in this work, and the emphasis of the current investigation was to study the effect of Zr^{4+} substitution on the performance of high rate and cycle stability.

Experimental

Material preparation

$Li_4Ti_{5-x}Zr_xO_{12}/C$ (x=0, 0.05) composites were prepared by a solution method. $LiOH{\cdot}H_2O$, $Zr(SO_4)_2{\cdot}4H_2O$, $Ti(OC_4H_9)_4$, and sucrose were used as reactants. Stoichiometric amounts of $LiOH{\cdot}H_2O$ and $Zr(SO_4)_2{\cdot}4H_2O$ were dissolved in distilled water to obtain solution A. $Ti(OC_4H_9)_4$ was dissolved in ethanol to obtain solution B. After the solution A and the solution B were mixed, adequate amount of sucrose was added into the solution. The solution was heated and maintained at 80 °C under vigorous stirring until the solvent evaporated. The product was dried at 80 °C for 12 h and yielded white precursors. The white precursors was calcined at 750 °C for 8 h in an argon atmosphere and then cooled in the furnace to room temperature.

Material characterization

The crystal structures of $Li_4Ti_{5-x}Zr_xO_{12}/C$ (x=0, 0.05) were characterized by X-ray diffraction (XRD, Rigaku D/MAX-RC) with Cu Kα radiation (λ=1.5405 Å, 45.0 kV, 50.0 mA). Elemental compositions of these samples (Ti, Zr) were determined by inductively coupled plasma optical emission spectroscopy (ICP-OES) (Perkin-Elmer optima 5300 DV). The content of carbon was determined through instrument (Elementar Analysensysteme GmbH). The morphology of particle was observed using a field emission scanning electron microscope (Quanta 200F, FEI) and a field emission transmission electron microscope (Tecnai G2F30). The particle size distribution was identified by laser particle size analyzer (OMEC LS900). The electrochemical characterizations were measured by charging and discharging over a voltage range of 0–2.5 V at different rates. The C rate was calculated from the weight and theoretical capacity of $Li_4Ti_5O_{12}$. Cyclic voltammetry measurements were performed using a CHI604C electrochemical working station at a scanning rate of 0.1 mV s^{-1}. Ac impedance measurement was carried out using a 5.0-mV ac voltage signal in the 100 KHz to 10 mHz frequency range in automatic sweep mode from high to low frequency.

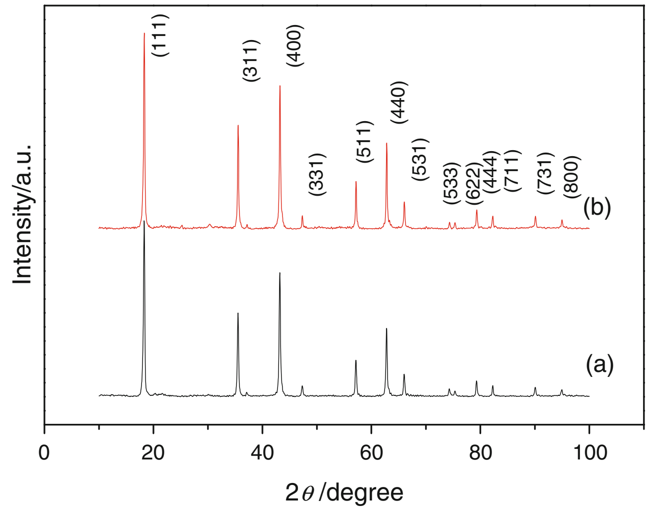

Fig. 1 XRD patterns of *a* $Li_4Ti_5O_{12}/C$ and *b* $Li_4Ti_{4.95}Zr_{0.05}O_{12}/C$

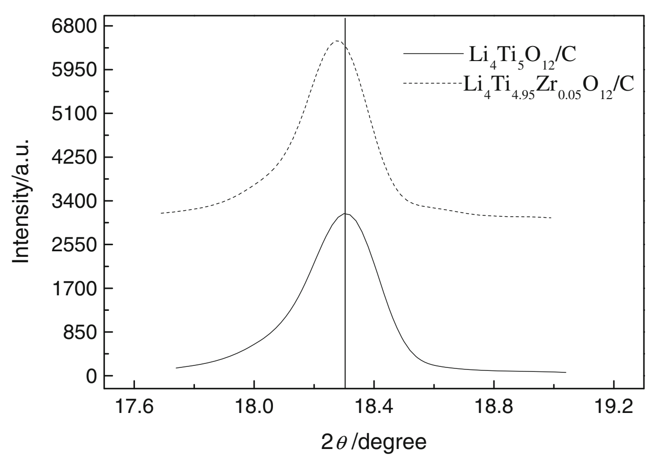

Fig. 2 Enlarged XRD patterns of (111) peaks of $Li_4Ti_5O_{12}/C$ and $Li_4Ti_{4.95}Zr_{0.05}O_{12}/C$ samples

Preparation of lithium-ion batteries

The working electrodes were prepared by spreading the anode slurry (80 wt.% of the active material, 10 wt.%

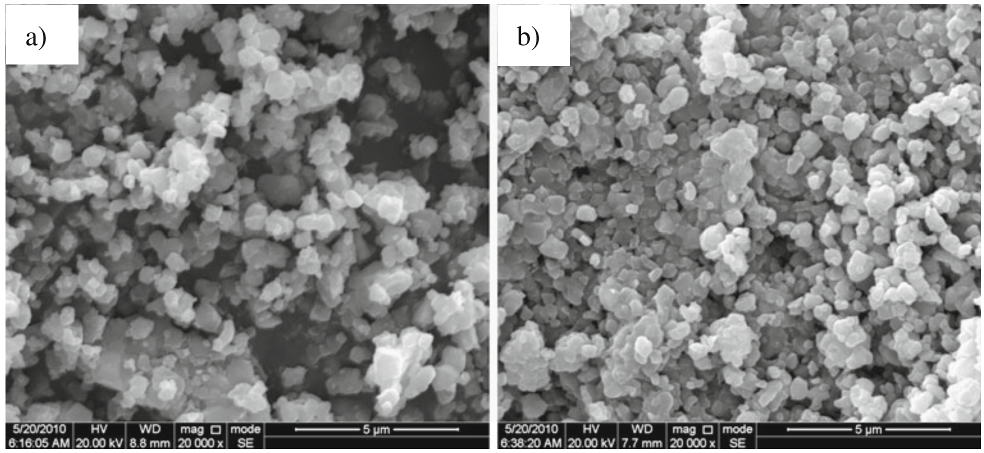

Fig. 3 SEM pictures of **a** $Li_4Ti_5O_{12}/C$ and **b** $Li_4Ti_{4.95}Zr_{0.05}O_{12}/C$

of polyvinylidene fluoride in *N*-methyl pyrrolidone, and 10 wt.% of carbon black) onto an copper foil followed by drying in vacuum at 120 °C for 12 h. A typical electrode disk contained 2.0–2.3 mg active material. The cells (CR2025) were assembled in an argon-filled glove box using lithium metal foil as the counter electrode. The electrolyte was 1.0 mol dm^{-3} $LiPF_6$ in a mixture of ethylene carbonate and dimethyl carbonate (1:1, *v*/*v*).

Results and discussion

Crystalline structure analysis

From the ICP-OES results, the ratio of Zr to Ti of $Li_4Ti_{4.95}Zr_{0.05}O_{12}/C$ was 0.048:4.92. The XRD patterns of the prepared products $Li_4Ti_5O_{12}/C$ and $Li_4Ti_{4.95}Zr_{0.05}O_{12}/C$ were shown in Fig. 1. All the diffraction peaks that could be indexed as spinel structure (cubic phase, space group *Fd3*m) were in accordance with JCPDS card no. 26-1198 without any impurity, indicating that the two kinds of materials exhibited pure phase of $Li_4Ti_5O_{12}$ with a spinel structure. The sharp peaks in the patterns showed good crystallinity of both electrode materials. The lattice parameters were calculated through the least square program method from the diffraction data of $Li_4Ti_5O_{12}/C$ and $Li_4Ti_{4.95}Zr_{0.05}O_{12}/C$ and were found to be 8.3572 Å and 8.3588 Å, respectively. The increase of the unit cell volume was because the ionic size of Zr^{4+} (0.080 nm) was bigger than that of Ti^{4+} (0.068 nm) [28].

Close inspection on the XRD patterns revealed that the peaks underwent a slight shift toward lower degrees with the doping of Zr^{4+}. For a clear observation, the peak position variation of (111) plane was magnified and shown in Fig. 2. It suggested that the zirconium ions were successively substituted for titanium(16*d*) in the $Li_4Ti_5O_{12}/C$ matrix structure. But no diffraction response of the carbon in XRD patterns was observed due to amorphous form and its low content. The result obtained from the elementary determinator indicated that the amount of carbon in the $Li_4Ti_5O_{12}/C$ and $Li_4Ti_{4.95}Zr_{0.05}O_{12}/C$ samples was about 2.4% and 2.3%, respectively.

Microstructure of the powders

Figure 3 showed the scanning electron microscopy (SEM) images of $Li_4Ti_5O_{12}/C$ and $Li_4Ti_{4.95}Zr_{0.05}O_{12}/C$. Figure 3a revealed that the particle of $Li_4Ti_5O_{12}/C$ was nonuniform

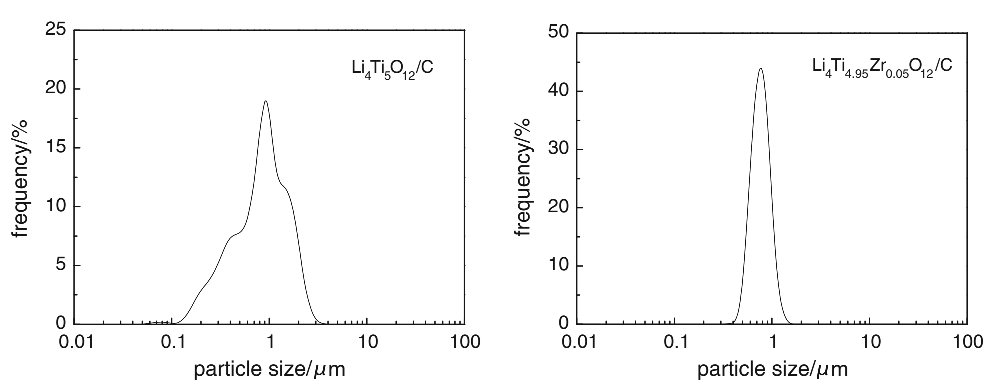

Fig. 4 The particle size distribution of $Li_4Ti_5O_{12}/C$ and $Li_4Ti_{4.95}Zr_{0.05}O_{12}/C$

Fig. 5 TEM pictures of **a** $Li_4Ti_5O_{12}$/C and **b** $Li_4Ti_{4.95}Zr_{0.05}O_{12}$/C

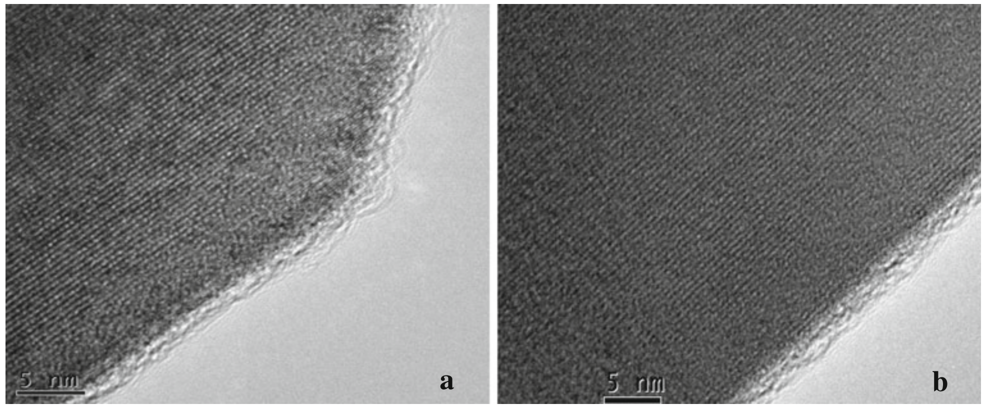

and partly formed slightly agglomerate particle. However, Fig. 3b showed that $Li_4Ti_{4.95}Zr_{0.05}O_{12}$/C had a uniform, nearly ball structural morphology with narrow size distribution. The small and uniform particle was good for contact between active materials and electrolyte; it was conducive to diffusion and transmission of lithium ions in the electrode. The particle size distribution of the undoped $Li_4Ti_5O_{12}$/C and $Li_4Ti_{4.95}Zr_{0.05}O_{12}$/C powers was depicted in Fig. 4. As shown in this figure, the average particle size of the $Li_4Ti_5O_{12}$/C and $Li_4Ti_{4.95}Zr_{0.05}O_{12}$/C powers was 0.98 and 0.67 μm, respectively. The result was in good agreement with the result of the SEM of the samples. It was evident that the Zr doping significantly decreased the particle size and degree of agglomeration of the product. In order to check carbon adhesion on the surface of $Li_4Ti_5O_{12}$/$Li_4Ti_{4.95}Zr_{0.05}O_{12}$ or dispersed in the powders, transmission electron microscopy (TEM) images were taken and were shown in Fig. 5. There were uniform carbon layers coating on the surface of $Li_4Ti_5O_{12}$/$Li_4Ti_{4.95}Zr_{0.05}O_{12}$ particles.

Electrochemical performance

To investigate the effect of dopant Zr on the electrochemical performance of the materials, $Li_4Ti_5O_{12}$/C and $Li_4Ti_{4.95}Zr_{0.05}O_{12}$/C were prepared anode materials of coin-type cells and the charge–discharge tests were studied. The charge–discharge curves were shown in Fig. 6, and the cycling performance was plotted in Fig. 7.

The rate of charge–discharge is 0.2C, and the potential range was from 0 to 2.5 V and 1 to 2.5 V vs. Li. It was evident that $Li_4Ti_{4.95}Zr_{0.05}O_{12}$/C had a higher capacity than $Li_4Ti_5O_{12}$/C at different discharge potential range. The capacity reached 373.44 mAh g^{-1} for the $Li_4Ti_{4.95}Zr_{0.05}O_{12}$/C discharge to 0 V, exceeding their theoretical capacities of 293 mAh g^{-1} [31].

These may be contributed from the intercalation and de-intercalation of lithium-ion in this low voltage range and the side reactions such as solid electrolyte interface layer formation on the surface of lithium titanate particles [19]. From the shape of the charge and discharge profiles, both the pure and substituted $Li_4Ti_5O_{12}$/C electrodes exhibited a plateau, respectively. The average charge voltage was around 1.57 V, while the discharge plateau was around 1.54 V. There was about 30 mV variance between the charge and discharge plateau, which was different from the observation of Ohuzuku [3] et al. It was probably caused by the different synthesis processes or different polarization of materials. In addition, $Li_4Ti_{4.95}Zr_{0.05}O_{12}$/C had a better

Fig. 6 Charge–discharge curves of *a* $Li_4Ti_5O_{12}$/C and *b* $Li_4Ti_{4.95}Zr_{0.05}O_{12}$/C, discharge to 0 and 1 V

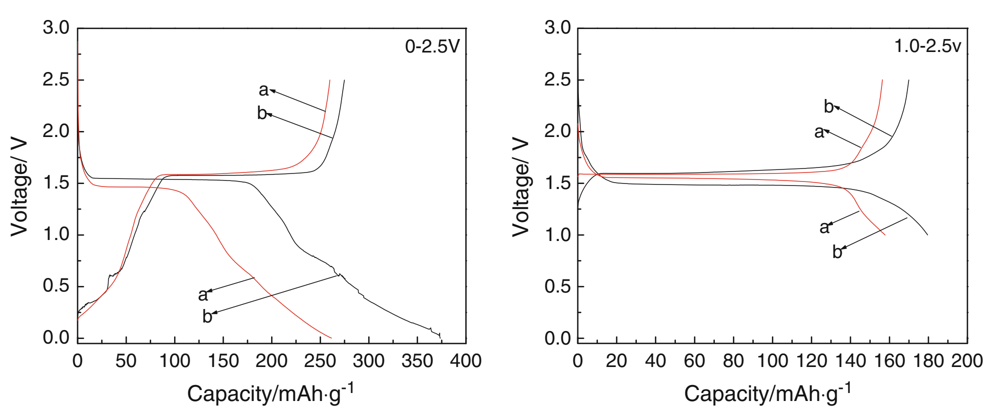

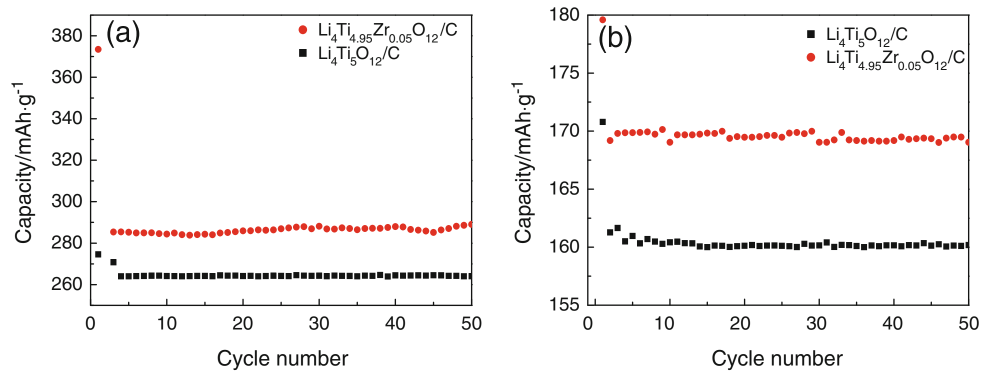

Fig. 7 Cycling performance of $Li_4Ti_5O_{12}$/C and $Li_4Ti_{4.95}Zr_{0.05}O_{12}$/C discharge to **a** 0 V and **b** 1 V

cycling performance than that of $Li_4Ti_5O_{12}$/C, which was related of the Zr^{4+} doping. It might be concluded that Zr^{4+} ions could enter the $Li_4Ti_5O_{12}$/C host structure which restrained undesirable particle growth and agglomerations. Although discharged to 0 V, the stability of materials was not affected. It might be attributable to the Zr^{4+} ions; these Zr^{4+} ions entering into the $Li_4Ti_5O_{12}$/C host structure stabilized the spinel structure by reducing the change of the structural framework during cycling. The electronic conductivity of the doped $Li_4Ti_5O_{12}$/C was improved by observing the preferable discharge capacity and cycling performance. It has been reported that the electronic conductivity of $Li_4Ti_5O_{12}$/C can be increased when Zr ions were successively substituted in the $Li_4Ti_5O_{12}$/C host structure [18]. The conductivities of $Li_4Ti_5O_{12}$/C and $Li_4Ti_{4.95}Zr_{0.05}O_{12}$/C powders were measured with the four-electrode method. The conductivity of $Li_4Ti_5O_{12}$/C can reach 5.4×10^{-6} S cm^{-1}, and $Li_4Ti_{4.95}Zr_{0.05}O_{12}$/C showed the higher electronic conductivity, reaching to 2.9×10^{-5} S cm^{-1}.All the results indicated that Zr^{4+} substitution has significantly improved the reversible capacity and cycling performance of the $Li_4Ti_5O_{12}$/C material.

Figure 8 showed the cyclic stability and high rate discharge ability of the samples $Li_4Ti_{5-x}Zr_xO_{12}$/C (x=0, 0.05) at 0.2C, 0.5C, 1C, 2 c, and 5C discharged to 0 V. The charge–discharge processes of the cell were taken for ten cycles at 0.2C, 0.5C, 1C, 2C, and 5C respectively. The discharge capacity of $Li_4Ti_{4.95}Zr_{0.05}O_{12}$/C was higher and the cyclic performance was better than those of $Li_4Ti_5O_{12}$/C. The discharge capacity of 284.67 mAh g^{-1} was obtained after tenth cycle at 0.2C, and the value was reduced to 263.20, 243.20, 229.36, and 212.61 mAh g^{-1} at the rate of 0.5C, 1C, 2C, and 5C, respectively. The cycleability of the $Li_4Ti_{4.95}Zr_{0.05}O_{12}$/C at 5C rate was shown in Fig. 9. Even after 200 cycles, the capacity retention was about 91.10% at the high rate of 5C. These phenomena indicated that Zr doping enhanced its rate capacity and cycle stability. It attributed to Zr doping sample having smaller particle size and less particle agglomeration than undoped $Li_4Ti_5O_{12}$/C. The results showed that Ti ions were successively substituted by Zr ion in the $Li_4Ti_5O_{12}$/C host structure. Smaller particle size and less particle agglomeration could reduce the distance of lithium-ion diffusion and augment the contact surface of electrode/electrolyte, which improved the electronic conductivity of the electrodes and lowered the electrode polarization at high rate, resulting in good cycle stability and high rate performance.

To better understand the electrochemical behaviors of $Li_4Ti_{5-x}Zr_xO_{12}$/C (x=0, 0.05), cyclic voltammetry was tested, as given in Fig. 10. The voltage was scanned from 0 to 3 V and then back to 0 V at the rate of 0.1 mV s^{-1}. The figure clearly exhibited that two samples had similar two pairs of redox peaks. It implied that Zr^{4+} doping did not change the electrochemical reaction process of $Li_4Ti_5O_{12}$/C in the voltage range of 0–3 V. But their intensities of the redox peaks were different. The intensities of the redox peaks for $Li_4Ti_{4.95}Zr_{0.05}O_{12}$/C were much higher than that of $Li_4Ti_5O_{12}$/C, indicating the higher electrochemical reactivity of Zr^{4+}-substitution electrodes. Furthermore,

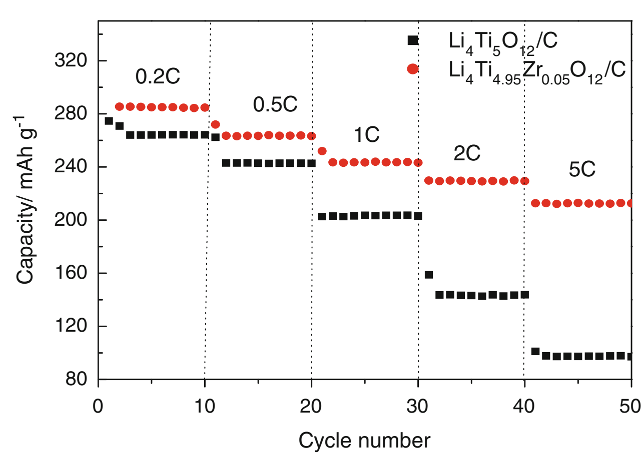

Fig. 8 Cycle performance of $Li_4Ti_5O_{12}$/C and $Li_4Ti_{4.95}Zr_{0.05}O_{12}$/C samples at different rate

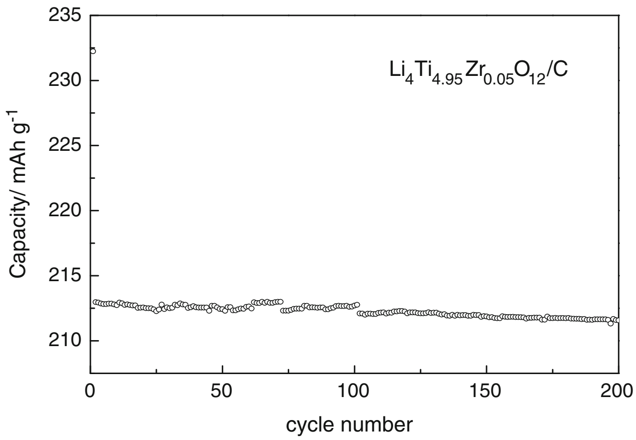

Fig. 9 The cycle performance of $Li_4Ti_{4.95}Zr_{0.05}O_{12}/C$ sample at 5C rate

the peak profiles of $Li_4Ti_{4.95}Zr_{0.05}O_{12}/C$ were more symmetric and sharp. $Li_4Ti_{4.95}Zr_{0.05}O_{12}/C$ exhibited an anodic peak at 1.696 V and a corresponding cathodic response at 1.491 V, whereas that of $Li_4Ti_5O_{12}/C$ is 1.703 V and 1.423 V, respectively. The potential intervals of $Li_4Ti_{4.95}Zr_{0.05}O_{12}/C$ and $Li_4Ti_5O_{12}/C$ are 0.205 and 0.280 V reversibility. As for cyclic voltammetry, the potential interval between anodic peak and cathodic peak was an important parameter to value the electrochemical reaction reversibility [32]. The sharp and symmetrical peaks appeared at around 1.45 and 1.70 V could be attributed to the redox of Ti^{4+}/Ti^{3+}. The reduction and oxidation peaks below 0.6 V could be proposed to another change of Ti^{4+} to Ti^{3+}, which suggested a multi-step restore of Ti^{4+} during the discharge potential down to 0 V [9]. In addition, values of the CV peaks were listed in

Table 1 Values of the CV peaks for $Li_4Ti_5O_{12}/C$ and $Li_4Ti_{4.95}Zr_{0.05}O_{12}/C$ samples

Samples	φ_{pa} (V)	φ_{pc} (V)	$\Delta\varphi_p$ (mV)
$Li_4Ti_5O_{12}/C$	1.703	1.423	280
$Li_4Ti_{4.95}Zr_{0.05}O_{12}/C$	1.696	1.491	205

Table 1. The potential differences between anodic and cathodic peaks for $Li_4Ti_5O_{12}/C$ and $Li_4Ti_{4.95}Zr_{0.05}O_{12}/C$ were 280 and 205 mV, respectively, suggesting the lower electrode polarization and higher lithium-ion diffusivity in solid-state body of sample $Li_4Ti_{4.95}Zr_{0.05}O_{12}/C$. These phenomena further confirmed that the doping of Zr^{4+} was beneficial to the reversible intercalation and de-intercalation of lithium ion in this synthesized anode material.

In order to further research the resistance and the electrochemical reaction properties of electrodes, we applied the ac impedance technique to monitor changes in electrolyte/LTO interface resistance at 0.2C rate upon cycling. The open-circuit voltages were about 3.0 V when the cells were in the initial state. Figure 11 showed the electrochemical impedance spectra of $Li_4Ti_5O_{12}/C/Li$ and Zr^{4+}-doped $Li_4Ti_5O_{12}/C/Li$ cells. The impedance spectra of the cells showed a depressed semicircle in the high middle frequency region and an oblique straight line in the low frequency region. The high middle frequency region of the semicircle represented the ohmic resistance of the cell, and the semicircle in the high middle frequency region was normally related to the complex reaction process over the electrolyte/anode, which might also include the particle contact resistance, charge-transfer resistance, and

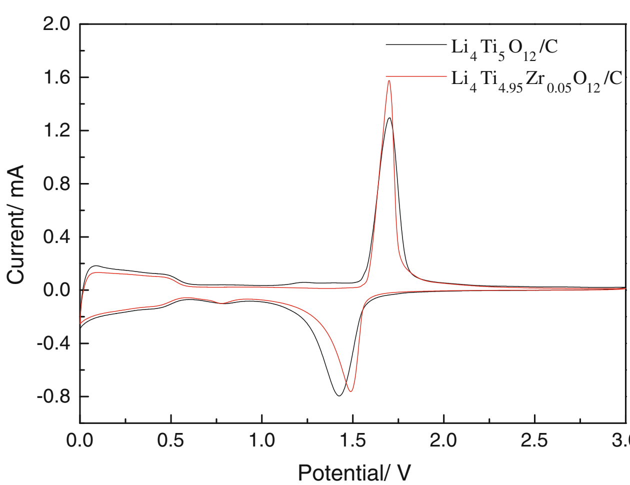

Fig. 10 Cycle voltammograms of cells using the $Li_4Ti_5O_{12}/C$ and $Li_4Ti_{4.95}Zr_{0.05}O_{12}/C$ sample as electrode materials

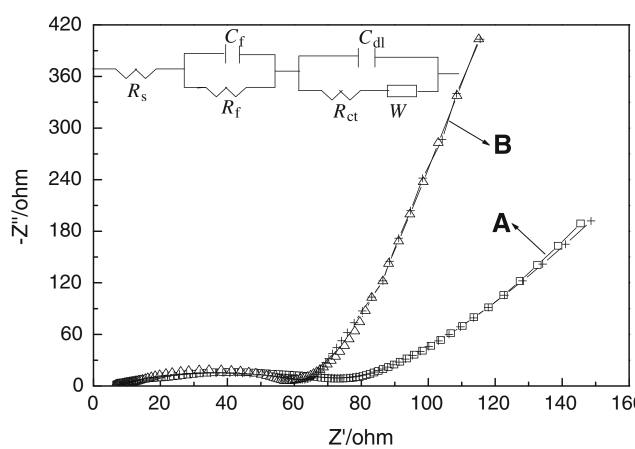

Fig. 11 AC impedance spectra of *a* $Li_4Ti_5O_{12}/C$ and *b* $Li_4Ti_{4.95}Zr_{0.05}O_{12}/C$ electrodes measured at open-circuit potential ~3.0 V vs. Li/Li^+

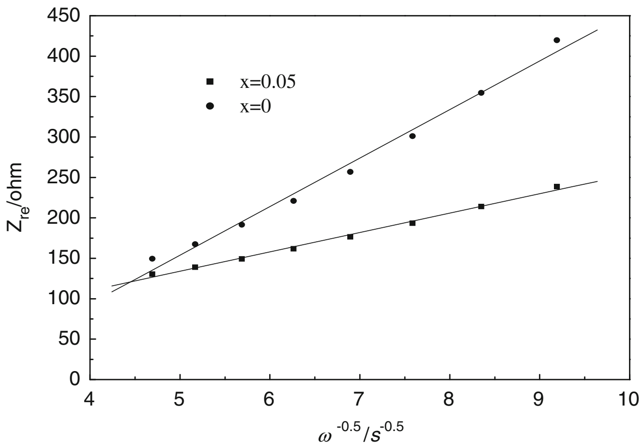

Fig. 12 Relationship between real impedance with the low frequency for the $Li_4Ti_{5-x}Zr_xO_{12}/C$ (x=0, 0.05) electrodes

corresponding capacitances. The low frequency region of the straight line was corresponding to the diffusion of the lithium ions into the bulk of the anode material of the so-called Warburg diffusion [33, 34].

To study the change in the ac impedance spectra of $Li_4Ti_5O_{12}$/C/Li and Zr^{4+}-doped $Li_4Ti_5O_{12}$/C/Li cells, we employed equivalent circuits to analyze the impedance spectra data, which were depicted in Fig. 11. In this fitted equivalent circuit, R_s was the ohmic resistance of electrolyte and electrode; R_{ct} was the charge-transfer resistance at the active material interface. R_f was the polarization resistance related with surface charge/discharge process and contacting resistance between anode particles. C_{dl} was the constant phase-angle element, attributed to double layer capacitance. C_f indicated the surface capacitance. Z_w represented the Warburg impedance reflecting the solid-state diffusion of Li ions into the bulk of the anode material. The plot of the real axis Z_{re} vs. the reciprocal square root of the lower angular frequencies $\omega^{-0.5}$ was illustrated in Fig. 12. From Fig. 12, we could obtain the value of Warburg impedance coefficient (σ_w). According to the following equations [35, 36]:

$$Z_{re} = R_s + R_{ct} + \sigma_w \omega^{-0.5}$$

$$D = \frac{R^2T^2}{2A^2n^4F^4C^2\sigma^2}$$

Where A is the area of the electrode surface, n the number of electron transfer, and C the molar concentration of Li^+ (moles per cubic centimeter), the lithium ion diffusion coefficient D could be obtained. The parameters of the equivalent circuit were shown in Table 2. From this table, it was obvious that R_{ct} was smaller for the $Li_4Ti_{4.95}Zr_{0.05}O_{12}$/C than that for $Li_4Ti_5O_{12}$/C electrode, which indicated that Zr^{4+} substitution could enable the charge-transfer much easier at the electrode/electrolyte interface and therefore decrease the overall battery internal resistance. This should be ascribed to the fact that the Zr-doped $Li_4Ti_5O_{12}$/C sample had smaller particle size and less particle agglomerations than the $Li_4Ti_5O_{12}$/C sample without Zr doping. At the same time, the value of Li chemical diffusion coefficient inside $Li_4Ti_{4.95}Zr_{0.05}O_{12}$/C electrode was bigger than inside $Li_4Ti_5O_{12}$/C electrode. It suggested that Zr ions had significant effect on the Li^+ transportation inside the electrode. So, the Zr^{4+}-doped $Li_4Ti_5O_{12}$/C had a higher capacity and better cycling stability at different voltage ranges.

Conclusions

Carbon-coated $Li_4Ti_{4.95}Zr_{0.05}O_{12}$ and $Li_4Ti_5O_{12}$ were successfully prepared by solution method. Both samples had good crystallinity and high phase purity. Zr^{4+} doping and carbon coating did not affect the spinel structure, and the doped sample had a smaller particle size and more regular morphological structure than those of $Li_4Ti_5O_{12}$/C. The electrochemical reaction process had not been changed by Zr doping. The electrochemical performance of $Li_4Ti_{4.95}Zr_{0.05}O_{12}$/C was evidently improved. The discharge capacity reached 289.03 mAh g^{-1} after 50 cycles for the Zr^{4+}-doped $Li_4Ti_5O_{12}$/C while it decreased to 264.03 mAh g^{-1} for the $Li_4Ti_5O_{12}$/C at the 0.2C discharge to 0 V, and the discharge capacities were 212.6 and 97.07 mAh g^{-1} with C rates of 5C, respectively. The capacity retention was about 91.10% at the high rate of 5C. It was clear that Zr^{4+}-doping sample enhanced the capacity retention and cycle stability especially at high charge–discharge rates, meanwhile the electrode of $Li_4Ti_{4.95}Zr_{0.05}O_{12}$/C had lower polarization and higher lithium-ion diffusivity. The Zr^{4+} doping improved surface reaction kinetics. It was beneficial to the reversible intercalation and de-intercalation of Ti^{4+} by Zr^{4+} substitution.

Table 2 The impedance parameters of the $Li_4Ti_{5-x}Zr_xO_{12}/C$ (x= 0, 0.05) electrodes

Sample	R_s (Ω)	R_f (Ω)	R_{ct} (Ω)	σ_w(Ω $cm^2/s^{0.5}$)	D(cm^2/s)
$Li_4Ti_5O_{12}$/C	7.26	49.68	71.94	60.02	3.97×10^{-12}
$Li_4Ti_{4.95}Zr_{0.05}O_{12}$/C	4.75	28.79	58.29	23.98	2.49×10^{-11}

Acknowledgments This work was supported by the National Science Foundation of China (project no. 20871036) and the Development Program for Outstanding Young Teachers in Harbin Institute of Technology (HITQNJS.2009.001).

References

1. Masatoshi M, Satoshi U, Eriko Y, Keiji K, Shinji I (2001) J Power Sources 101:53–59
2. Ding N, Fang X, Xu J, Yao YX, Zhu J, Chen CH (2009) J Appl Electrochem 39:995–1001
3. Ohuzuku T, Ueda A, Yamamoto N (1995) J Electrochem Soc 142:1431–1435
4. Thackeray MM (1995) J Electrochem Soc 142:2558–2563
5. Guerfi A, Sévigny S, Lagacé M, Hovington P, Kinoshita K, Zaghib K (2003) J Power Sources 119:88–94
6. Aurelien Du, Pasquier HCC, Spitler T (2009) J Power Sources 186:508–514
7. Guerfi A, Charest P, Kinoshita K, Perrier M, Zaghib K (2004) J Power Sources 126:163–168
8. Li X, Qu MZ, Yu ZL, Chinese (2010) J Inorg Chem 26:233–239
9. Chen CH, Vaughey JT, Jansen AN, Dees DW, Kahaian AJ, Goacher T, Thackeray MM (2001) J Electrochem Soc 148:102–104
10. Zhang B, Hongda Du, Li B, Kang F (2010) Electrochem Solid-State Lett 13:36–38
11. Robertson AD, Trevino L, Tukamoto H, Irvine JTS (1999) J Power Sources 81–82:352–357
12. Zhao H, Li Y, Zhu Z, Lin J, Tian Z, Wang R (2008) Electrochim Acta 53:7079–7083
13. Martlń P, López ML, Pico C, Veiga ML (2007) Solid State Sci 9:521–526
14. Robertson AD, Tukamoto H, Irvine JTS (1999) J Electrochem Soc 146:3958–3962
15. Hao YJ, Lai QY, Lu JZ, Ji XY (2007) Ionics 13:369–373
16. Huang SH, Wen ZY, Zhu XJ, Lin ZX (2007) J Power Sources 165:408–412
17. Zhong Z (2007) Electrochem Solid-State Lett 10:A267–A269
18. Li X, Qu M, Yu Z (2009) J Alloys Compd 487:L12–L17
19. Yi TF, Shu J, Zhu YR, Zhu XD, Yue CB, Zhou AN, Zhu RS (2009) Electrochim Acta 54:7464–7470
20. Yi TF, Shu J, Zhu YR, Zhu XD, Zhu RS, Zhou AN (2010) J Power Sources 195:285–288
21. Allen JL, Jow TR, Wolfenstine J (2006) J Power Sources 159:1340–1345
22. Qi YL, Huang YD, Jia DZ, Bao SJ, Guo ZP (2009) Electrochim Acta 54:4772–4776
23. Huang S, Wen Z, Gu Z, Zhu X (2005) Electrochim Acta 50:4057–4062
24. Huang SH, Wen ZY, Lin B, Han JD, Xu XG (2008) J Alloys Compd 457:400–403
25. Huang S, Wen Z, Zhang J, Gu Z, Xu X (2006) Solid State Ionics 177:851–855
26. Cheng L, XiLi L, HaiJing L, HuanMing X, PingWei Z, YongYao X (2007) J Electrochem Soc 154:A692–A697
27. Yuan TY, Cai X, Zhou R, Shao YK (2010) J Power Sources 195:4997–5004
28. Wu HsienChang Wu, HungChun LE, NaeLih Wu (2010) Electrochem Commun 12:488–491
29. Chengmin S, Xiaogang Z, Yingke Z, Hulin L (2002) Mater Chem Phys 78:437–441
30. Fattakhova D, Petrykin V, Brus J, Kostlánová T, Dědeček J, Krtil P (2005) Solid State Ionics 176:1877–1885
31. Ge H, Li N, Li D, Dai C, Wang D (2009) J Phys Chem C 113:6324–6326
32. Ni JF, Zhou HH, Chen JT, Zhang XX (2005) Mater Lett 59:2361–2365
33. Huang JJ, Jiang ZY (2008) Electrochim Acta 53:7756–7759
34. Huang SH, Wen ZY, Zhu XJ, Lin ZX (2005) J Electrochem Soc 152:A186–A190
35. Li J, Jin YL, Zhang XG, Yang H (2007) Solid State Ionics 178:1590–1594
36. Shenouda AY, Liu HK (2009) J Alloys Compd 477:498–503